A study of H/D plasma fuelling in the H-1 heliac using optical coherence imaging techniques

J. Howard, B. Blackwell, C. Michael, A. Wang

Plasma Research Laboratory, Australian National University , Canberra, A.C.T., 0200 Australia

SUMMARY

Because of its coil-in-tank design, particle fuelling issues are very significant for plasma peformance in the H-1 heliac. We have studied the temporal and spatial evolution of hydrogen and deuterium relative abundances by applying coherence imaging methods for the observation of Hβ and Dβ emissivities. Such methods may also be useful for estimating relative abundances of hydrogen isotopes in the divertor regions of fusion devices.

The plasma light emission is processed by an electro-optically modulated fixed-delay polarization interferometer which monitors the coherence (phase and amplitude) of the beat interferogram resulting from the superposition of the Hβ and Dβ light.

Because the coherence is encoded at harmonics of the electro-optic modulation frequency, a single detector array suffices to deliver time-resolved images of both Hβ and Dβ emissivities.

.

MEASUREMENT PRINCIPLE

The MOSS spectrometer monitors the interferogram phase and contrast at one or more fixed delays using frequency domain multiplexing techniques. Consider the Gaussian spectral line

$$I(\nu) = I_0 \exp\left[-(\nu - \nu_0)^2/2\sigma^2\right]$$

Its interferogram is written as

$$S = I_0(1 + \zeta \cos \phi_0)$$

with fringe contrast

$$\zeta = \exp\left(-\sigma^2 \phi_0^2 \kappa^2 / 2\nu_0^2\right)$$

and $\phi_0 = 2\pi\nu_0 LB_0/c$ is the birefringent plate phase delay. B_0 is the birefringence at optical frequency ν_0. L is the plate thickness and κ accounts for the birefringence dispersion.

When the intensity ratio of a line pair changes, the spectral centre of mass shifts, giving rise to a change in the interferometric phase shift and contrast. The intensity ratio is thus ``calculated'' directly by the instrument. The total interferogram can be written as

$$S = I_1(1 + \zeta_1 \cos o_1) + I_2(1 + \zeta_2 \cos o_2)$$

$$\dot{} = \tfrac{\omega}{4} I[\psi^{1/4} + \zeta \widehat{\cos}(o_0^{1/4} \tfrac{\Delta\nu}{\nu_0} \eta)]$$

The separate line-integrated component intensities can also be unfolded using just a single detector element per viewing sightline, obviating the need for relative channel sensitivity calibration. It can be shown that

$$I = I_1 + I_2$$

$$I\zeta \cos\eta = (I_1\zeta_1 + I_2\zeta_2)\cos\delta$$

$$I\zeta \sin\eta = (I_1\zeta_1 - I_2\zeta_2)\sin\delta$$

where I, ζ and η are obtained from the MOSS system. These equations allow the recovery of the unknown component intensities. Sensitivity depends on the difference phase parameter determined by the spectral line separation $\Delta\nu$ and the birefringent delay ϕ_0 (See Figs 3 and 4):

$$\delta = (\phi_1 - \phi_2)/2 = \phi_0\kappa \frac{\Delta\nu}{\nu_0} \equiv \hat{\phi}_0 \frac{\Delta\nu}{\nu_0}$$

This approach opens the way for time-resolved imaging of relative isotope abundances, electron temperatures or other physical parameters upon which the intensity ratio is dependent.

APPARATUS

The MOSS camera has been described in detail elsewhere. It has been used extensively for the study of ion temperatures and flows in the H-1 heliac.

A recent improvement has been to replace the interference filter used for isolating the spectral region of interest with a high-throughput low-resolution grating spectrograph. The MOSS polarization interferometer and imaging optics form an image of the plasma onto a 16-element linear multi-anode photomultiplier tube array located in the spectrograph image plane. The trapezoidal instrument response is shown in Fig. 3.
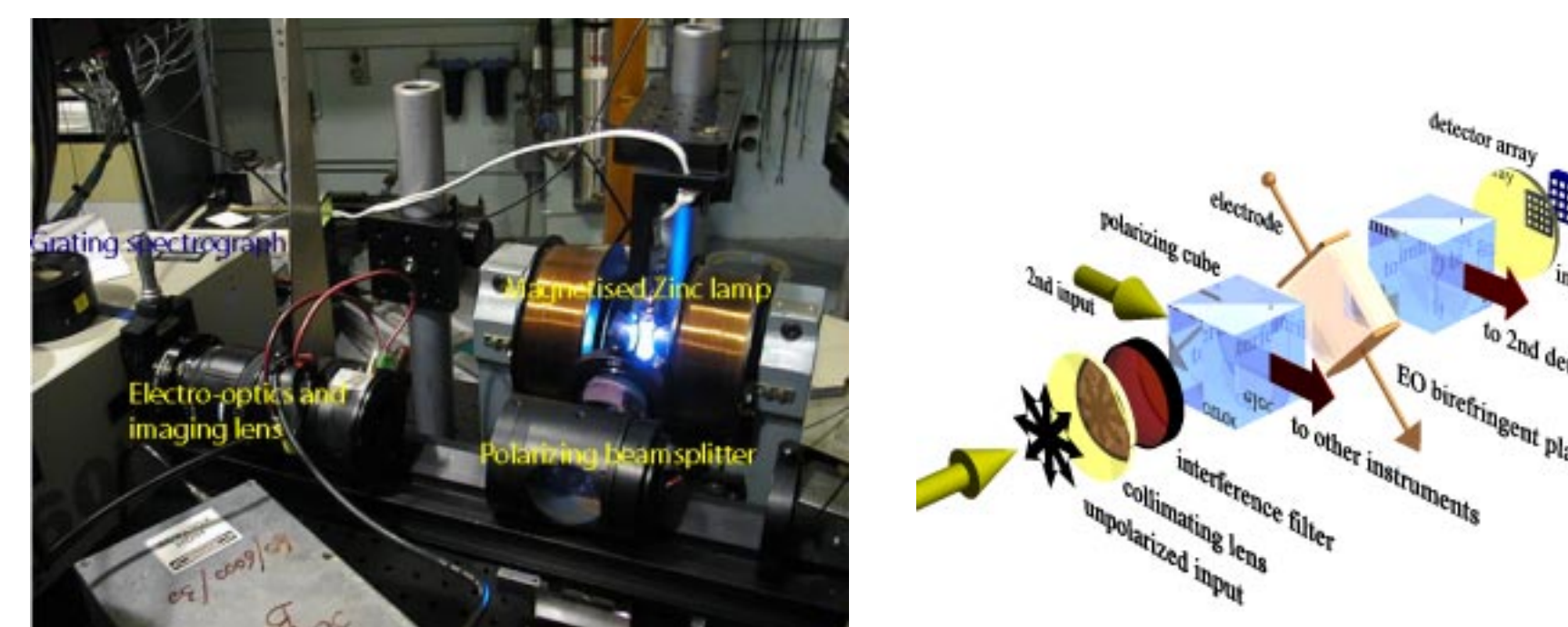

Fig. 1. Left: Layout of the coherence imaging system. The light is collimated by an objective lens before passing the polarizing beamsplitter cube. Following the poalrizer, the light traverses an electrooptically modulated birefringent LiNbO3 plate (0-100 kHz), a final polarizer, and is imaged through a low-resolution grating spectrograph onto a linear multi-anode photomultiplier array. Right: Schematic depiction of imaging MOSS components

ZEEMAN CALIBRATION MEASUREMENTS

We have used the normal Zeeman effect to confirm the imaging and dispersive properties of the MOSS camera. The variation of the line splitting $\Delta\nu$ with magnetic field strength gives rise to a beating of the component interferograms and a subsequent sinusoidal modulation of the fringe contrast.
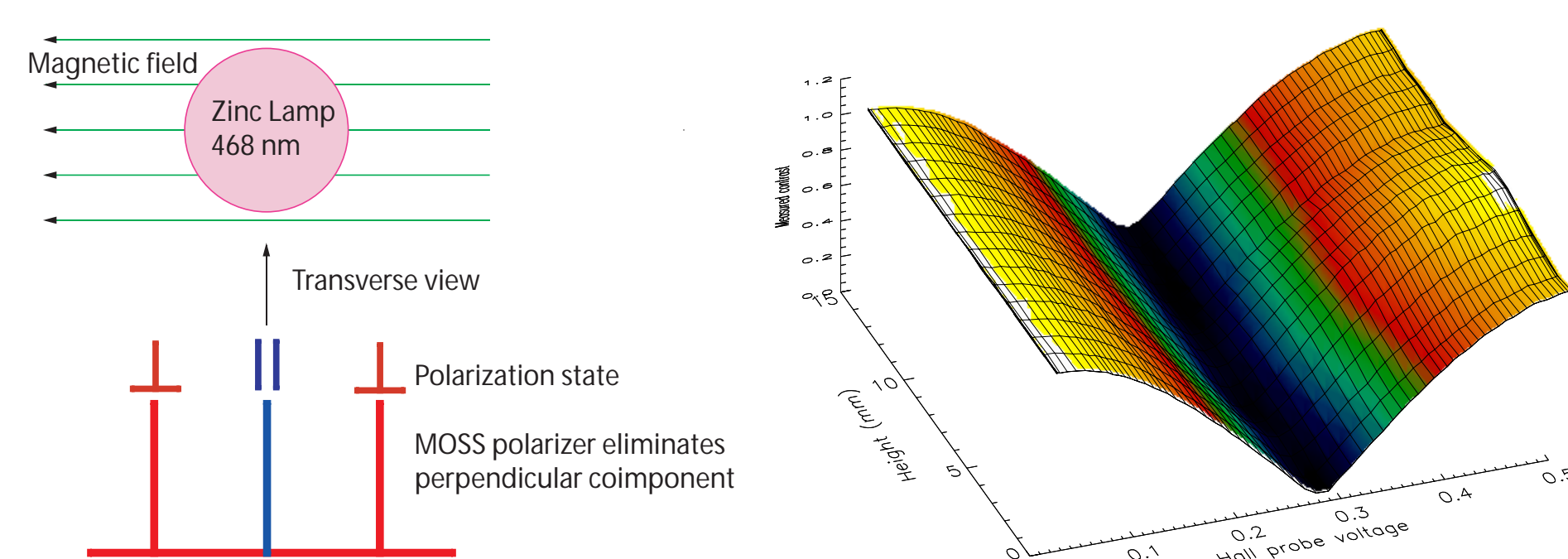

Fig. 2. Left: The polarizer admits the s polarization components whose separation increases with magnetic field strength. Right: By monitoring the interference pattern contrast at a fixed optical delay it is possible to image the contraction in the beat period due to the increasing frequency separation of the Zeeman doublet with magnetic field.

EXPERIMENTS ON H-1

We report preliminary results obtained in resonantly heated 0.5T, (60 kW, 7MHz) plasmas in mixtures of hydrogen and deuterium. The experiments were obtained for an on-axis rotational transform of 0.31 and with controlled variation of the filling partial pressures, keeping the total pressure approximately constant.
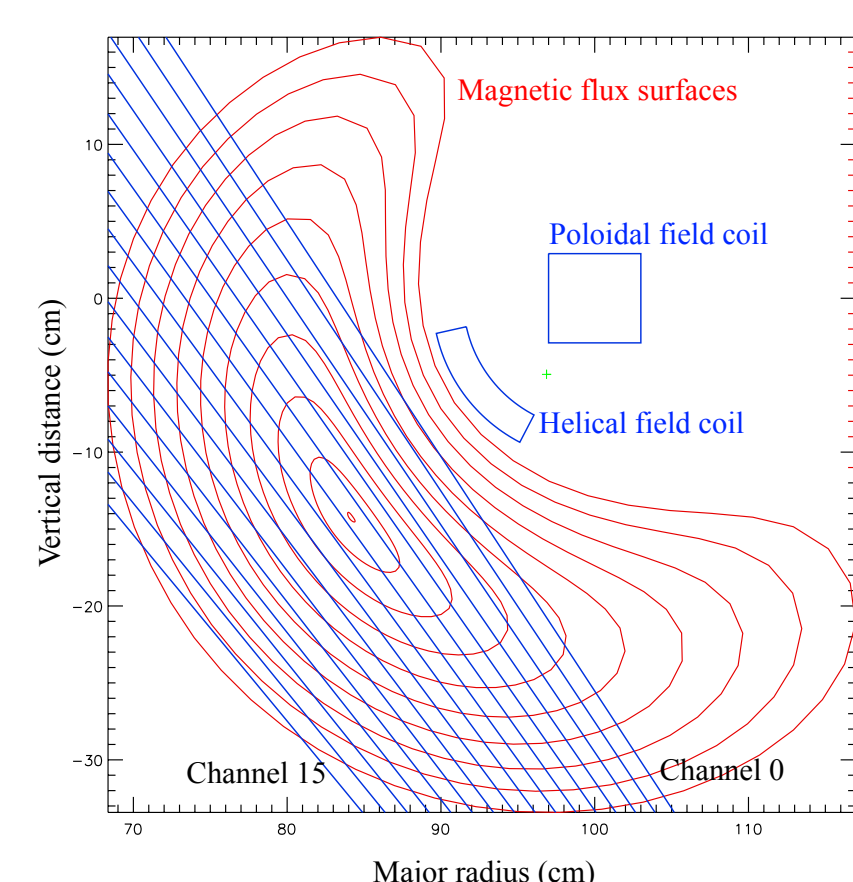

Fig. 3. Schematic of the plasma cross section showing helical control winding and MOSS camera lines of sight.

SIMULATION RESULTS

The measured spectrum (Fig 3) allow us to calculate the expected variation of fringe contrast and phase with relative intensity (H/D ratio) for a lithium niobate delay plate of thickness 5mm (vertical line in Fig. 4). The figure shows that the phase and contrast variations are linked and can unambiguously resolve the intensity ratio.
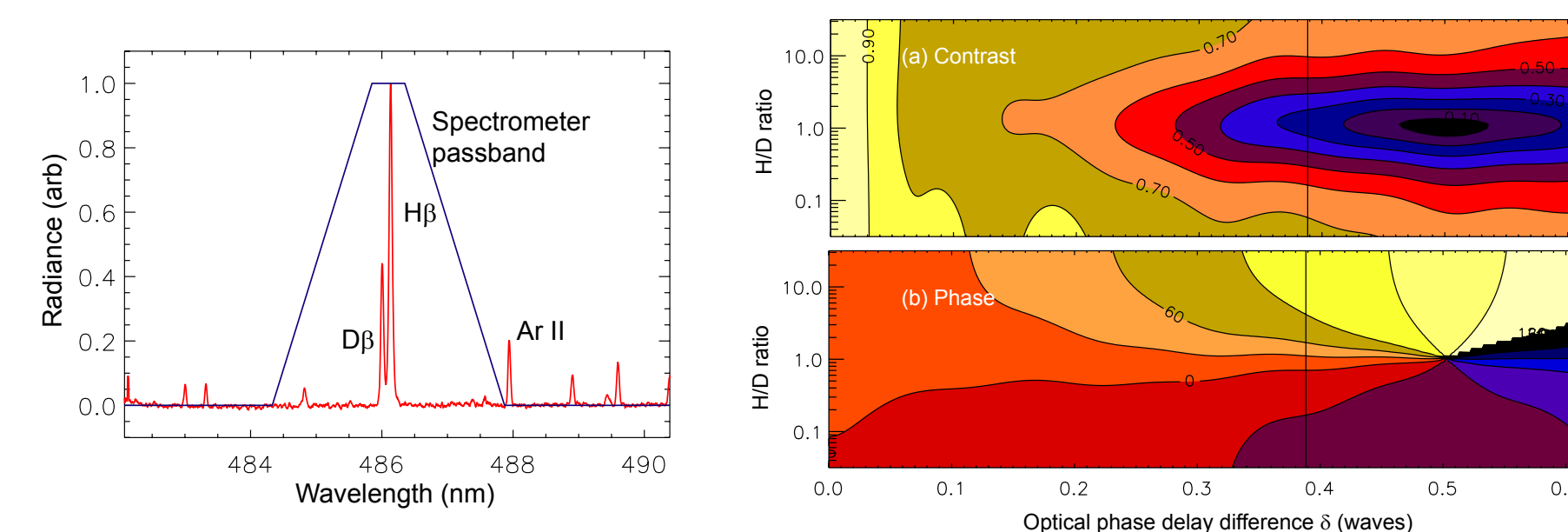

Fig. 4. Left: A representative, spectrum showing Hβ and Dβ spectral lines in relation to the grating spectrometer passband. There is some low level contamination by Ar II lines and continuum background.
Right: Variation of interferogram contrast (top) and phase (below) as a function of H/D ratio (vertical axis) and optical delay difference. The contrast is a minimum (zero) when the line intensities are identical (maximum linewidth). At the contrast minimum, the phase also shifts by half a wave as either H or D dominates the spectrum. The vertical line corresponds to the delay introduced by a the 5mm. thick lithium niobate plate used in these experiments.L ow-level irregularites are produced by contaminating lines within the spectral passband.

DEPENDENCE ON SPECTRAL LINEWIDTH

The modelling shows that when broadening σ is significant compared with line separation $\Delta\nu$ there is an optical delay difference δ for which sensitivity to intensity ratios is optimized. At this delay, relative isotope abundance (first spectral moment) can be sensitively determined, even when thermal broadening is much greater than the spectral line separation. For our experiments, Hβ and Dβ are well resolved and the optimum optical delay, which is obtained using a birefringent plate, is chosen to be close to the first node of the beat interferogram.
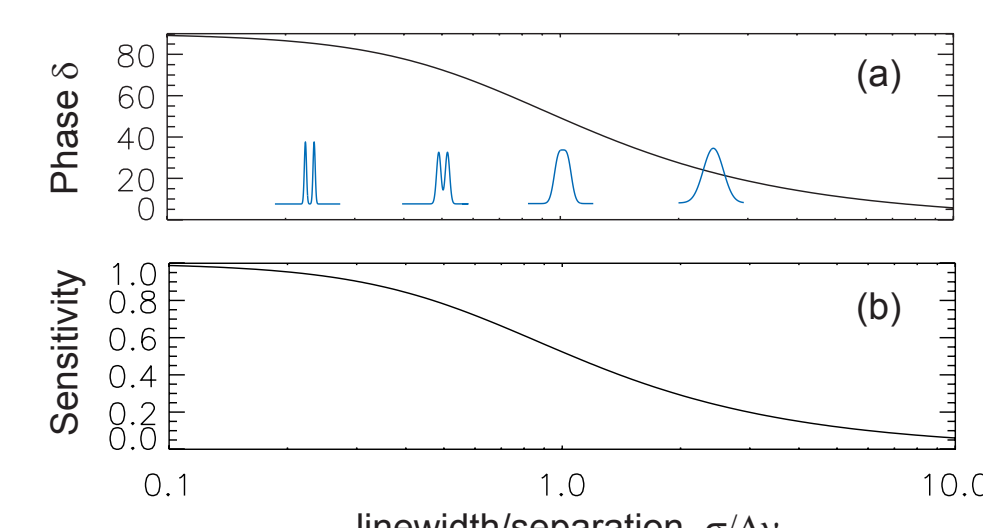

Fig. 5. (a) The variation of optimum difference phase delay δ (degrees) with linewidth to separation ratio $\sigma/\Delta\nu$. (b) the relative sensitivity of the measurement to changes in the emission intensity ratio. The blue curves indicate the blurring of the lineshape as a function of the parameter $\sigma/\Delta\nu$.
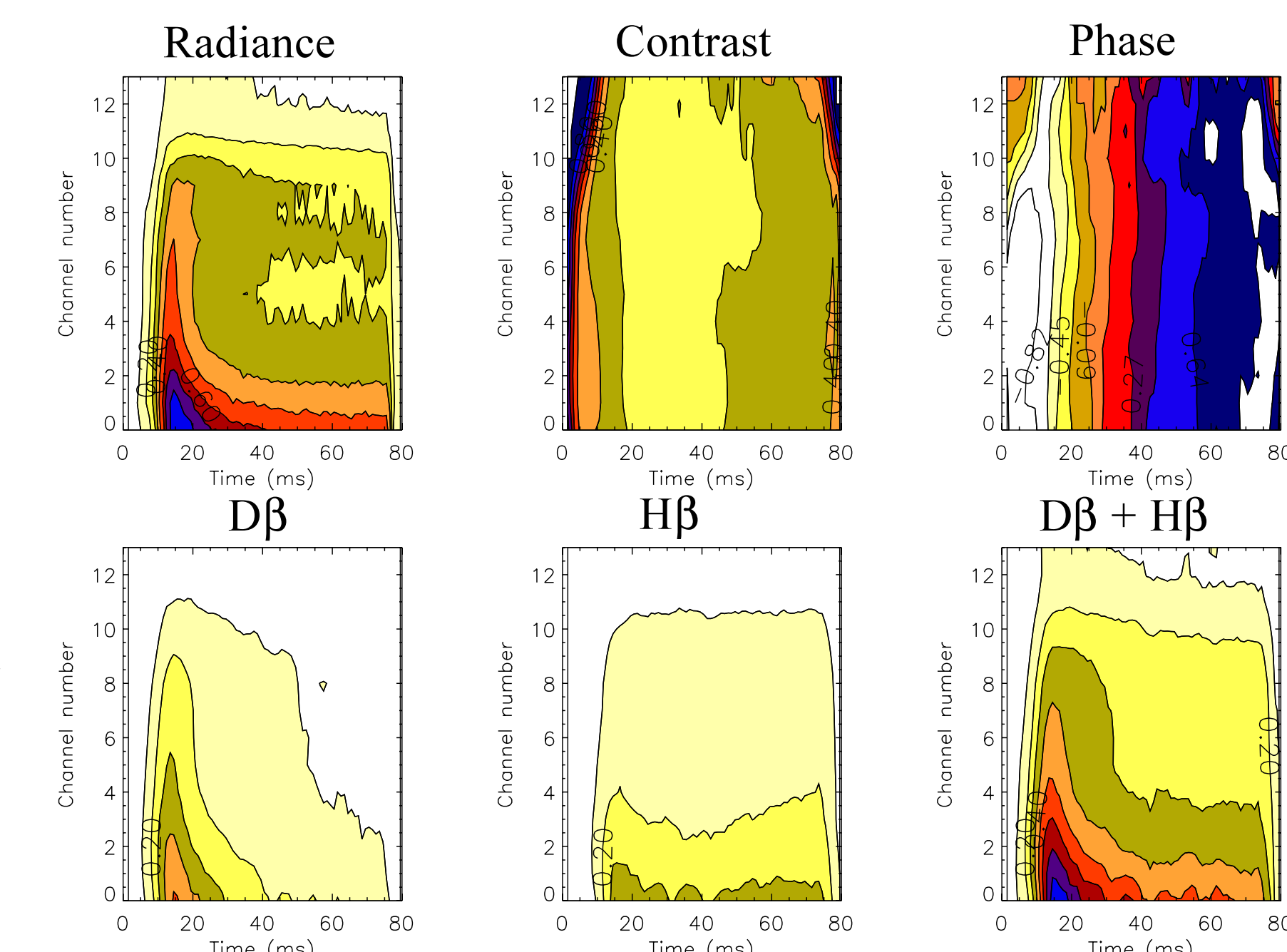
EXPERIMENTAL RESULTS

Fig. 6. Top row L to R: The temporal and spatial variation of the total radiance, contrast and phase obtained using the MOSS camera. The major radius of the viewing lines increases with channel number. The emission is much brighter for chords viewing adjacent to the inner helical ring conductor. Notice that the contrast decreases to a minimum at 40ms (equal radiance for both H and D) and then increases. The phase continues to ramp linearly, indicating that one of the species (hydrogen) becomes dominant.
Bottom row L to R: the unfolded deuterium and hydrogen components, and their sum. The latter matches well the measured total radiance.
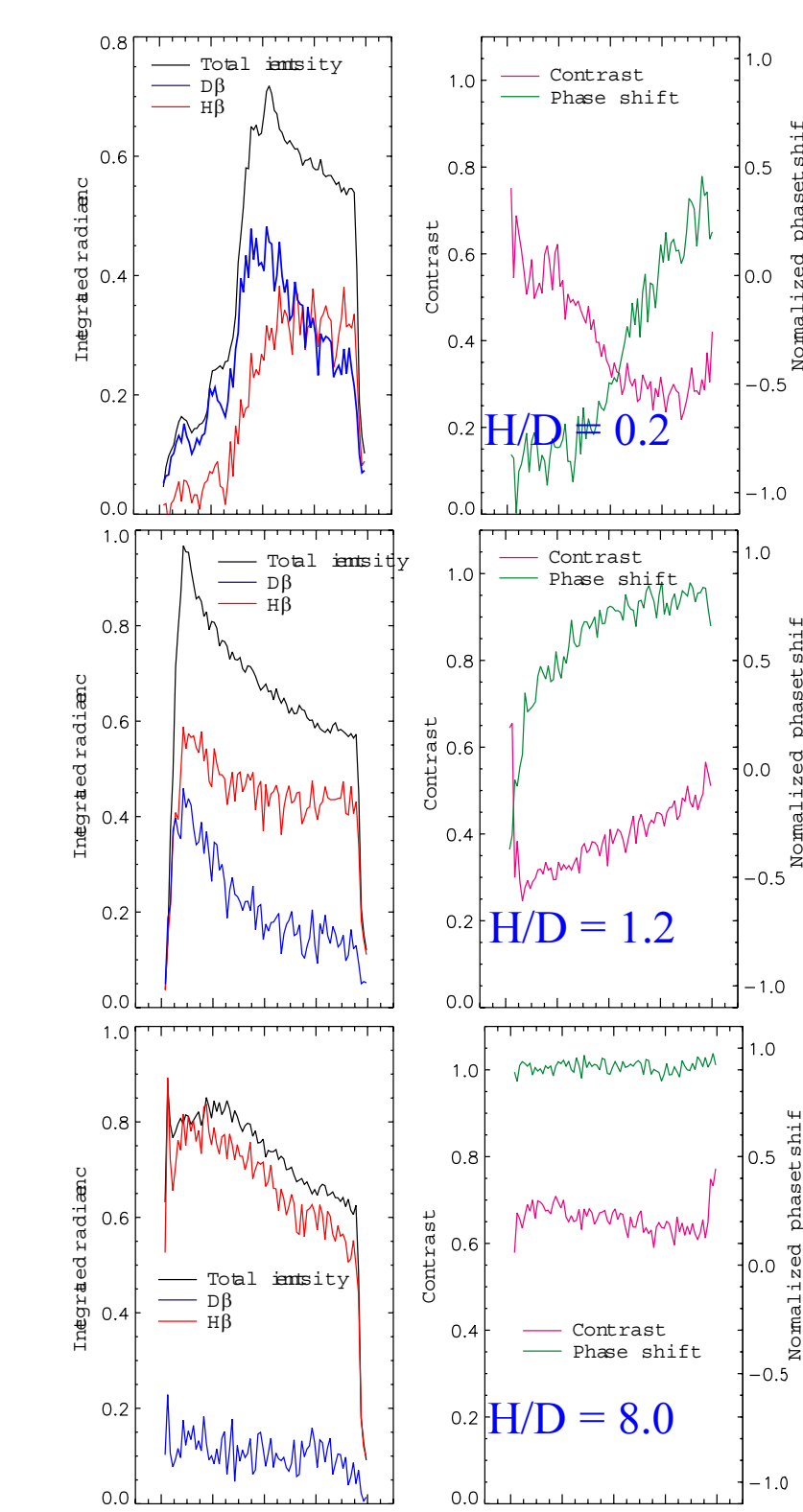
EXPERIMENTAL RESULTS (CONTINUED)

Fig. 7. Left: Temporal evolution of the three intensity components at camera channel 0 (See Fig. 3)
Right: Interferogram phase and contrast.
Top: Partial pressure fraction H/D = .02
Centre: Partial pressure fraction H/D = 1.2
Bottom: Partial pressure fraction H/D = 8.0

The phase shift has been normalized to the difference phase δ. Time varying interferometric phase indicates that the relative intensities of hydrogen and deuterium emission are changing.

When the relative line intensities change, the interferogram contrast and phase are constrained to lie on the the curve

$$\frac{\zeta}{\zeta_2}\sin(\delta - \eta) \mid \frac{\zeta}{\zeta_2}\sin(\eta \mid \delta) = \sin 2\delta$$
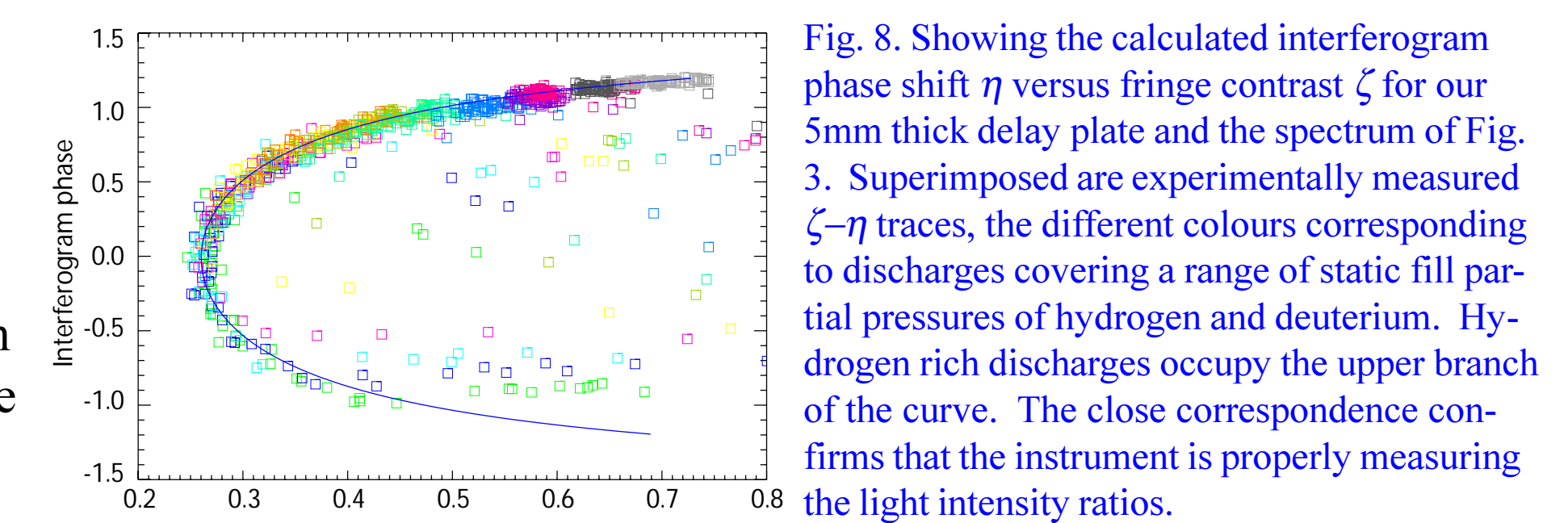

Fig. 8. Showing the calculated interferogram phase shift η versus fringe contrast ζ for our 5mm thick delay plate and the spectrum of Fig. 3. Superimposed are experimentally measured ζ-η traces, the different colours corresponding to discharges covering a range of static fill partial pressures of hydrogen and deuterium. Hydrogen rich discharges occupy the upper branch of the curve. The close correspondence confirms that the instrument is properly measuring the light intensity ratios.
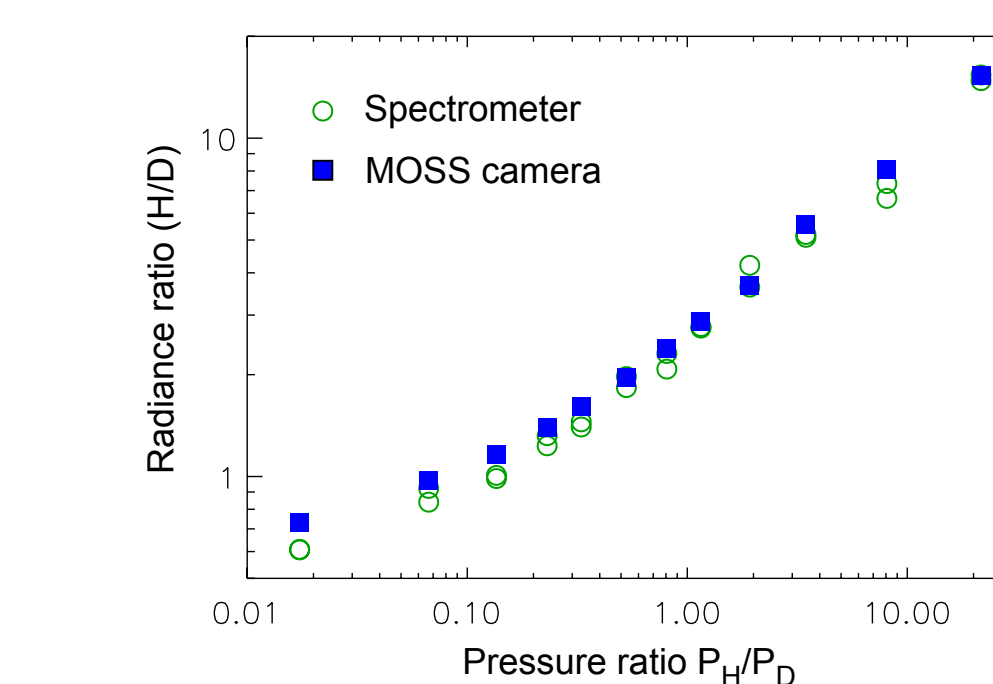

Fig. 9. The ratio of spatially and temporally integrated component light intensities measured using the MOSS camera compared with temporally integrated spectral ratio obtained using a grating spectrometer.
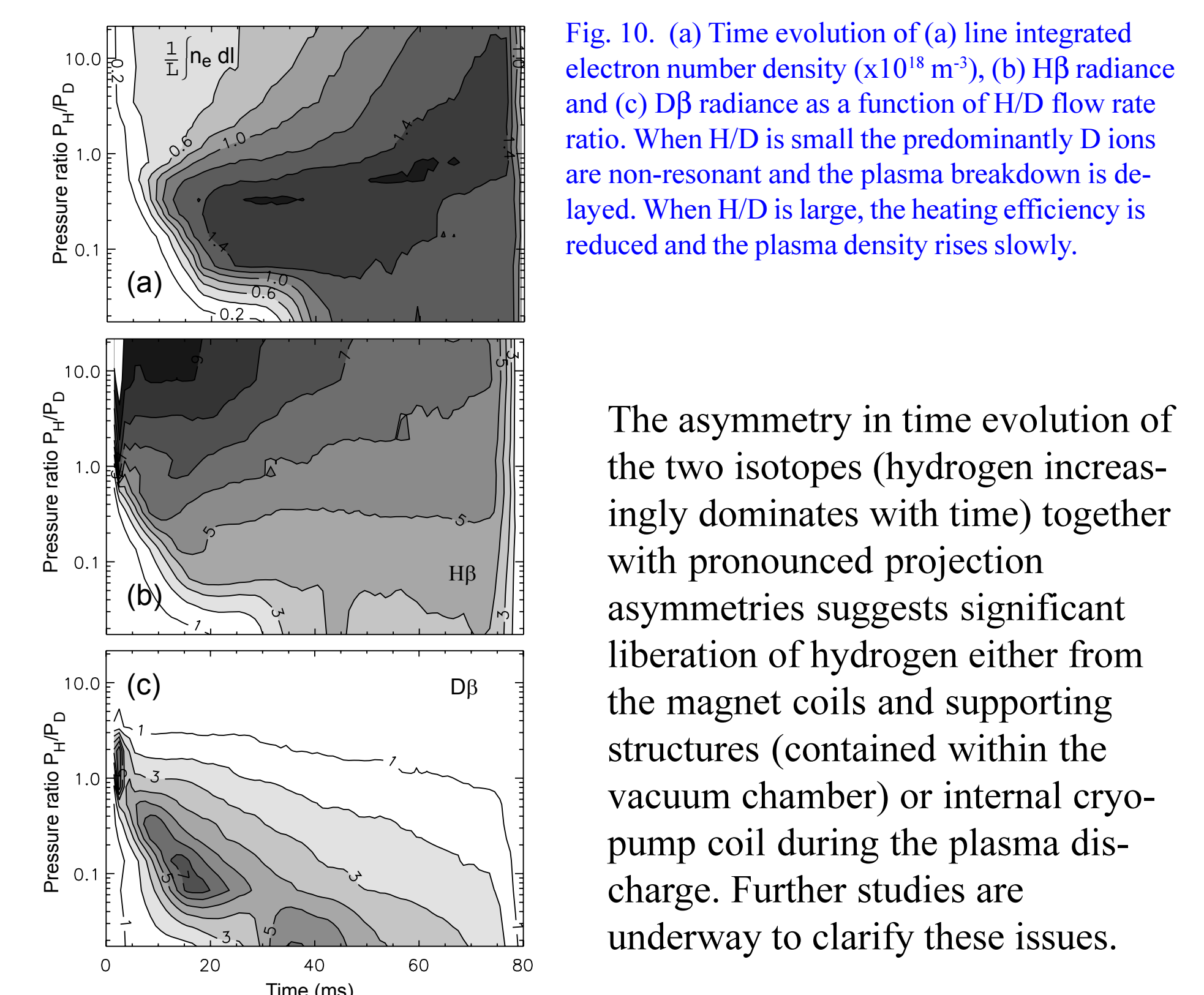

Fig. 10. (a) Time evolution of (a) line integrated electron number density (x10^18 m-3), (b) Hβ radiance and (c) Dβ radiance as a function of H/D flow rate ratio. When H/D is small the predominantly D ions are non-resonant and the plasma breakdown is delayed. When H/D is large, the heating efficiency is reduced and the plasma density rises slowly.

The asymmetry in time evolution of the two isotopes (hydrogen increasingly dominates with time) together with pronounced projection asymmetries suggests significant liberation of hydrogen either from the magnet coils and supporting structures (contained within the vacuum chamber) or internal cryopump coil during the plasma discharge. Further studies are underway to clarify these issues.